Am J Transl Res 2022;14(7):4948-4963
www.ajtr.org /ISSN:1943-8141/AJTR0141128

Original Article

Hsa_circular RNA_0001013 exerts oncogenic effects in gastric cancer through the microRNA-136-TWSG1 axis

Zhaofeng Gao[1,2*], Lingyu Hu[2*], Fei Chen[2], Chunhua He[2], Biwen Hu[2], Xiaoguang Wang[1,2]

[1]*Faculty of Graduate Studies, Zhejiang Chinese Medical University, Hangzhou 310053, Zhejiang, P. R. China;*
[2]*Department of Surgery, The Second Affiliated Hospital of Jiaxing University, Jiaxing 314000, Zhejiang, P. R. China.*
[*]*Equal contributors.*

Received December 14, 2021; Accepted June 8, 2022; Epub July 15, 2022; Published July 30, 2022

Abstract: Background: Gastric cancer (GC) is one of the leading malignancies of the digestive system. Circular RNAs (circRNAs) are well-established to play critical regulatory roles in GC development. The current study sought to explore the effects and regulatory mechanism of circ_0001013 in the course of GC. Methods: First, differential circRNAs and related mechanisms in GC were predicted by microarray analysis. Circ_0001013, microRNA (miR)-136, and TWSG1 expression patterns were subsequently detected in GC clinical samples and cells using RT-qPCR. The relationship among circ_0001013, miR-136, and TWSG1 was further assessed by dual-luciferase reporter assay, biotin-coupled probe pull-down assay, and biotin-coupled miRNA capture. Based on gain- and loss-of-function assays, GC cell proliferation, migration, invasion, and the cell cycle and apoptosis were also measured by 5-ethynyl-2'-deoxyuridine (EdU) assay, scratch test, Transwell assay, and flow cytometry, respectively. Moreover, the effect of circ_0001013 on tumor growth was detected by tumor xenografting in nude mice. Results: Circ_0001013 was predicted to be up-regulated in GC by microarray profiling, which was confirmed by RT-qPCR detection in GC tissues and cells. miR-136 was poorly expressed, and TWSG1 was highly expressed in GC tissues. Mechanistically, circ_0001013 bound to miR-136, which negatively targeted *TWSG1* in the GC cells. Silencing circ_0001013 or *TWSG1* or over-expressing miR-136 led to decreased GC cell proliferation, migration, invasion, and cell cycle arrest and enhanced apoptosis. Furthermore, silencing circ_0001013 resulted in diminished *TWSG1* expression and inhibited transplanted tumor growth in the nude mice. Conclusion: Collectively, our findings indicated that circ_0001013 increased TWSG1 expression by binding to miR-136, thereby exerting oncogenic effects in GC.

Keywords: Gastric cancer, Circ_0001013, miR-136, TWSG1, migration, invasion, apoptosis

Introduction

With more than 1 million new cases and 784,000 deaths reported in 2018, gastric cancer (GC) is the 5th leading cancer in morbidity and 3rd leading cause of cancer-related deaths across the globe [1]. A variety of risk factors can contribute to carcinogenesis of GC, including diets low in fruit and vegetables, *Helicobacter pylori* infection, high salt intake, and age [2]. Clinically, GC presents with a number of symptoms, such as nausea, early satiety, emesis, anorexia, weight loss, dyspepsia, and epigastric pain, all of which are vague, non-specific, and may not occur until latter disease stages [3]. Despite the numerous advancements made in the treatment of GC, the prognosis of advanced GC still remains extremely poor, exerting a burden on society and medical infrastructure [4]. A heterogeneous disease and the endpoint of a long and multistep process, GC is precipitated by the gradual accumulation of various (epi)genetic alterations, resulting in an imbalance of oncogenic and anti-oncogenic pathways [5]. Accordingly, our understanding of the mechanistic actions underlying GC may enable more personalized therapy and improve outcome.

The work of our peers has shown that noncoding RNAs (ncRNAs), such as circular RNAs (circRNAs), microRNAs (miRNAs, miRs), and long ncRNAs, are all implicated in the development of GC [6]. Moreover, circRNAs are known to play an oncogenic role in GC development *via* a circRNA-miRNA-mRNA network [7]. For instance,

circLMO7 induces GC progression by augmenting the proliferative, invasive, and migration capacities of GC cells through the miR-30a-3p-WNT2 axis [8]. In addition, hsa_circ_0001829 exerts an enhancing effect on GC cell proliferation, migration, and invasion, and simultaneously decreases cell cycle entry and apoptosis by the miR-155-5p-SMAD2 axis [9]. Further highlighting the influence of circRNAs, hsa_circ_0023409 was previously shown to regulate GC cell proliferation and metastasis by the miR-542-3p-IRS4 axis [10]. In a similar light, bioinformatics analyses in our previous investigation predicted the involvement of circ_0001013 in the pathogenesis of GC. Subsequently, we studied the downstream miRNA-mRNA mechanism of circ_0001013 in GC. On a separate note, over-expression of miR-136 is associated with elevation of human GC cell apoptosis [11]. However, there is a scarcity of investigations focusing on the interaction between circ_0001013 and miR-136. Furthermore, twisted gastrulation BMP signaling modulator 1 (*TWSG1*) is known to function as an oncogene in papillary thyroid cancer (PTC) [12]. However, the interaction between miR-136 and *TWSG1* in GC development has not been defined. In lieu of these, the current study carried out a series of tissue, cell, and animal experiments to determine whether the circ_0001013-miR-136-TWSG1 network could influence the development of GC.

Materials and methods

Ethics statement

Human inclusion and experimentation in the current study were approved by the Second Affiliated Hospital of Jiaxing University Ethics Committee (Approval number: 2016-19) and conformed to guidelines published in the *Declaration of Helsinki*. Signed informed consents were obtained from all participants prior to inclusion. Animal experiment procedures were performed in accordance with the ethical standards of the animal experiment system approved by the Jiaxing University Medical College Experimental Animal Ethics Committee (Approval number: JUMC2020-039). Extensive measures were taken to minimize the suffering of the included animals.

Bioinformatic analysis

First, the GSE83521 microarray dataset of GC-related circRNAs was retrieved from the Gene Expression Omnibus database. The obtained microarray data were pre-processed and normalized using the Affy package of R software [13]. The limma package [14] was adopted to screen differential circRNAs with *log2FC (fold change) > 1 or < -1 and P < 0.05* serving as the criteria, followed by heat mapping of the differential circRNAs. The possible regulatory mechanism of circ_0001013 was further predicted using the CircInteractome database. Additionally, GC-related miRNAs were downloaded from the MNDR v3.1 database (http://www.rna-society.org/mndr/), with "Gastric cancer" serving as the key word, and screening conditions of Species=Homo sapiens & Score > 0.6. Subsequently, we analyzed the KEGG pathways that miRNAs were involved in using the miRPathDB v2.0 database (https://mpd.bioinf.uni-sb.de/). Further, we queried the expression patterns of miR-136 and miR-638 in GSE16579 dataset (miRNA expression of human cancer and mouse cell lines) in the deepBase v3.0 database (http://rna.sysu.edu.cn/deepbase3/). Thereafter, GO enrichment analysis of the candidate genes was performed using the R language package "clusterProfiler" (https://bioconductor.org/packages/release/bioc/html/clusterProfiler.html). The target genes of miR-136 were further predicted with the miRDB (http://www.mirdb.org/), starBase (http://starbase.sysu.edu.cn/), DIANA-microT (http://diana.imis.athena-innovation.gr/DianaTools/index.php?r=microT_CDS/), and mirDIP databases (http://ophid.utoronto.ca/mirDIP/). Differentially expressed genes were analyzed based on GC samples from The Cancer Genome Atlas (TCGA) database employing the GEPIA (Gene Expression Profiling Interactive Analysis) tool. Afterwards, the intersection of analyzed miRNA-target genes and the differentially highly expressed genes in GC was obtained using the Jvenn tool (http://jvenn.toulouse.inra.fr/app/example.html). The survival curve was analyzed using the KMplot website (http://kmplot.com/).

Vector construction and dual-luciferase reporter assay detection of circ_0001013 target gene

Target genes of circ_0001013 were predicted using the CircInteractome database. Dual-luciferase reporter assay was performed to investigate whether miR-136 was a direct target gene of circ_0001013. The sequences were

obtained from the GenBank database (National Center for Biotechnology Information, Bethesda, MD, USA). In accordance with the prediction results, we designed the 3' untranslated region (UTR) sequence of miR-136 (the target gene of circ_0001013). Reporter gene plasmid vectors containing miR-136-3'UTR wild-type (Wt) and miR-136-3'UTR mutant-type (Mut) were subsequently cloned using one-step site-directed mutagenesis. Next, over-expression (oe)-circ_0001013 was co-transfected with miR-136-Wt or miR-136-Mut plasmids into cells for 24 h. After a 6-h period of conventional culture in a 5% CO_2 incubator at 37°C, the medium was replaced with new medium. After another 48 h period of continuous culture, the cells were lysed, after which 100 μL PLB was added to each well, shaken at low speed for 15 min, and set aside at -4°C. Dual-luciferase reporter assay was conducted in accordance with the provided instructions of the dual-luciferase reporter gene assay kit (#E1910, Hengsheng Biotechnology, Inner Mongolia, China) as follows: 100 μL fluorescein assay reagent II was added to a 1.5 mL Eppendorf tube and a TD20/20 luminometer (Turner Designs, Sunnyvale, CA, USA) was initiated to predict for 2 s. Cell lysis (20 μL) was added to the tube, mixed thoroughly, and the tube was placed in the luminometer to determine firefly luciferase (FLUC) activity. Thereafter, 100 μL Stop & Glo preparation was added to measure *Renilla* luciferase (RLUC) activity. Afterwards, the relative luciferase intensity was calculated based on the RLUC to FLUC ratio, which was also used to determine miRNA target sites.

Detection of dual-luciferase activity

Target genes of miR-36 were analyzed by online prediction (TargetScan, http://www.targetscan.org/vert_72/). Subsequent dual-luciferase reporter assay confirmed that *TWSG1* was a direct target of miR-136. *TWSG1* 3'UTR gene fragment was cloned into a pMIR-reporter. The sequenced Wt and Mut luciferase reporter plasmids were subsequently co-transfected with miR-136 into HEK-293T cells, which were lysed after 48-h transfection. Afterwards, the luciferase activity was estimated using a Dual-Luciferase Reporter Assay System (Promega, WI, USA).

Sample collection

GC tissues and adjacent normal tissues were collected from patients diagnosed with GC and undergoing surgery at the Second Affiliated Hospital of Jiaxing University from 2016 to 2019. None of the included patients received drug treatment prior to specimen collection. A total of 70 pairs of tissue samples were collected, immediately frozen in liquid nitrogen, and stored at -80°C.

Cell culture

Human 293T cells and GES-1 human normal gastric epithelial cells were cultured in Dulbecco's modified Eagle's medium (Thermo Fisher Scientific, Waltham, MA, USA). Simultaneously, human GC cell lines AGS, MKN74, MKN45, and HGC-27 were cultured in RPMI 1640 medium (Gibco, Carlsbad, CA, USA). Both media were supplemented with 10% fetal bovine serum (FBS, Gibco, Carlsbad, CA, USA), 100 U/mL penicillin, and 100 mg/mL streptomycin. All cells were subsequently cultured in a humidified incubator with 5% CO_2 at 37°C.

Reverse transcription-quantitative PCR (RT-qPCR)

Total RNA content was extracted from tissues or cells using the TRIzol reagent. Next, RNA concentration and purity were determined by spectrophotometry, and RNA integrity was assessed by agarose gel electrophoresis. miRNA-specific complementary DNA was synthesized by a TaqMan MicroRNA reverse transcription kit and the primers from a TaqMan MicroRNA Assay. miR-136 expression patterns were measured according to TaqMan miRNA Assay protocols and standardized to U6. The primers were synthesized by the Beijing Genomics Institute (BGI, Beijing, China) (**Table 1**). Reverse transcription was performed in accordance with the manufacturer's instructions of the EasyScript First-Strand cDNA Synthesis SuperMix kit (AE301-02, Beijing TransGen Biotech Co., Ltd., Beijing, China). Reaction solution was adopted for real-time fluorescent qPCR on a real-time fluorescent qPCR instrument (ABI 7500, ABI, Foster City, CA, USA), in accordance with the manufacturer's instructions of a SYBR® Premix Ex Taq™ II kit (Takara, Dalian, China). Afterwards, fold changes were calculated using the comparative threshold cycle ($2^{-\Delta\Delta Ct}$) method.

Western blot assay

Cells were lysed with radioimmunoprecipitation assay cell lysis buffer (P0013B, Beyotime,

Table 1. The RT-qPCR primers

Gene	Sequence (5'-3')
miR-136	Forward: 5'-ACTCCATTTGTTTTGATGATGGA-3'
	Reverse universal primer
U6	Forward: 5'-GCTTCGGCAGCACATATACTAAAAT-3'
	Reverse universal primer
circ_0001013	Forward: 5'-AGTGGGATGCCACAAGATCC-3'
	Reverse: 5'-AGTCATTCGCCGTTGATCGT-3'
TWSG1	Forward: 5'-GCTGTGCTTACTCTAGCCATC-3'
	Reverse: 5'-TGAGGCATTTGCTCACATCAC-3'
GAPDH	Forward: 5'-GGAGCGAGATCCCTCCAAAAT-3'
	Reverse: 5'-GGCTGTTGTCATACTTCTCATGG-3'

Note: RT-qPCR, reverse transcription-quantitative PCR; GAPDH, glyceraldehyde-3-phosphate dehydrogenase; miR-136, microRNA-136; circ_0001013, hsa_circular RNA_0001013; TWSG1, twisted gastrulation BMP signaling modulator 1.

Shanghai, China) containing phenylmethylsulphonyl fluoride at a final concentration of 1 mM. The proteins were quantified with a Bio-Rad DC Protein Assay kit (EWELL Bio-Technology Co., Ltd., Guangdong, China). Each sample was mixed with sodium dodecyl sulfate buffer and boiled for 10 min. Next, the samples were subjected to gel electrophoresis at 80 V for 30 min and 120 V for 90 min. Subsequently, the proteins were electrically imprinted from the gel onto a polyvinylidene fluoride membrane at a constant current of 300 mA for 90 min. The membrane was then blocked with Tris-buffered saline with Tween 20 containing 5% skimmed milk powder and shaken at 37°C for 2 h. The membrane was probed with primary antibodies (Abcam, Cambridge, UK) against TWSG1 (dilution ratio of 1:1000, ab218995, mouse) and glyceraldehyde-3-phosphate dehydrogenase (GAPDH, dilution ratio of 1:5000, ab8245, mouse anti-human) at 4°C for 12 h, followed by 1-h of re-probing with goat anti-rabbit immunoglobulin G secondary antibody (dilution ratio of 1:20,000, ab6721, Abcam). Afterwards, the blots were developed by sensitized enhanced chemiluminescence, and the gray value of the protein bands was measured using the ImageJ software (NIH, Bethesda, MD, USA).

Scratch test

Cells were cultured in a 6-well plate at a density of 2.5×10^4 cells/cm^2. After 24 h, the medium was aspirated, and a wound was made with a 10 μL sterilized disposable pipette. Next, the cells were rinsed twice with phosphate-buffered saline (PBS) and cultured in RPMI 1640 medium containing 10% FBS. Wound healing at 0 h and 48 h was observed at the same location. The migration of the GC cells was expressed as the migration rate: (scratch width at T_{48} - scratch width at T_0)/scratch width at $T_0 \times 100\%$.

Transwell assay

Apical chamber of a Transwell chamber (8-μm aperture, Costar, Cambridge, MA, USA) was coated with Matrigel (BD Biosciences, Franklin Lakes, NJ, USA). Transfected cells (at a density of 1×10^4 in 200 μL serum-free medium) were seeded into the upper chamber for invasion detection. Simultaneously, medium containing 10% FBS was added to the bottom chamber as a chemical attractant. Next, the cells were incubated at 37°C for 48 h to detect invasion in a 5% CO_2 chamber. Following incubation, the cells in the apical chamber were removed by cotton swabs and the cells on the lower surface were fixed with methanol, stained with 0.1% crystal violet, and finally observed under a microscope (× 200 magnification, Olympus, Tokyo, Japan).

Flow cytometry

Cells (1×10^6) were fixed with 70% cold ethanol, mixed with 1 mL propidium iodide (PI) staining solution (Becton Dickinson; 50 μg/mL), and then allowed to stand in the dark for 30 min. Next, the cell cycle was determined using a FACSCalibur flow cytometer, and the results were analyzed with the ModFit software.

Afterwards, cells (1×10^6) were resuspended in 1 × annexin buffer and stained with 5 μL annexin V-FITC (fluorescein isothiocyanate) (Becton Dickinson) and 1 μL PI in teh dark for 10 min. Next, the mixture was placed in the dark for 5 min. Afterwards, the cells were suspended with 300 μL 1 × annexin buffer and the results were analyzed by flow cytometry.

5-Ethynyl-2'-deoxyuridine (EdU) assay

GC cells in the NC group and the small interfering RNA (si)-circ_0001013 group were labeled with EdU as per the manufacturer's instruc-

tions of the EdU proliferation detection kit (CA1170, Solarbio, Beijing, China). After discarding the supernatant, 100 μL medium containing EdU (30 μmol/L) was added to each well for 12-h incubation. Next, the cells were fixed with 4% paraformaldehyde for 30 min, mixed with 50 μL 2 mg/mL glycine for 5 min, and then stained with 100 μL Apollo® staining solution in the dark, followed by nuclear staining with Hoechst 33342 (Thermo Fisher Scientific). Image-Pro software was utilized for image acquisition and quantitative analysis.

Biotin-coupled probe pull-down assay

The biotinylated probe sequence of circ_0001013 was 5'-FITC-GGACCGAGTCAAGTCAAAGG-3'. Cells (1×10^7) were lysed in lysis buffer and incubated with 3 μg biotinylated probe for 2 h at room temperature. Next, the cell lysate was cultured with streptavidin magnetic beads (Life Technology, Gaithersburg, MD, USA) for 4 h to pull down the biotin-coupled RNA complex. The magnetic beads were subsequently washed five times with lysis buffer and the miRNA in the complex was extracted with the TRIzol reagent for real-time qPCR.

Biotin-coupled miRNA capture

Cells (2×10^6) were lysed with 50 μm biotinylated miRNA mimic (sequence: GCCCTTCATGCTGCCCAG) at 50% aggregation state. After a 24-h period of transfection, the cells were lysed in lysis buffer, mixed with 50 μL streptavidin beads for 2 h, and then added to tubes to pull down the biotin-conjugated RNA complex. The tubes were subsequently incubated and rotated at a low speed (10 rpm) for 4 h on a rotator. Next, the beads were washed several times with lysis buffer, and RNA specifically interacting with miRNA was recovered with the TRIzol LS reagent (Life Technology). Afterwards, the abundance of circ_0001013 was assessed by RT-qPCR and agarose gel electrophoresis.

Northern blot assay

Northern blot assay was performed with northern blotting kits (Ambion, Austin, TX, USA). Briefly, total RNA was denatured in formaldehyde and electrophoresed with 1% agarose-formaldehyde gel. Next, the obtained RNA was transferred to a Hybond-N+ nylon membrane and hybridized with the biotin-labeled DNA probe. Binding RNA was subsequently detected using a biotin chromogenic assay kit. Later, the membrane was analyzed with the Image Lab software (Bio-Rad, Hercules, CA, USA).

Fluorescence in situ hybridization (FISH)

The circ_0001013 sequence and miR-136-specific probe were utilized for FISH. Cy5-labeled and farm-labeled probes were specifically targeted to circ_0001013 and miRNA, respectively. Next, the nuclei were stained with 4',6-diamidino-2-phenylindole. All steps were performed in accordance with the manufacturer's instructions. Images were captured using the Zeiss LSM 880 NLO confocal microscope system (Leica Microsystems, Mannheim, Germany).

Mouse xenografts

AGS cells (1×10^7) were subcutaneously injected into the left armpit of BALB/c nude mice (aged 4-6 weeks old, weighing 18-22 g; 8 mice per group) to establish a xenograft mouse model. After the tumors had grown to 100 mm^3, lentivirus containing sh-circ_0001013 (1×10^9 TU/ml, 50 μl) alone, or combined with agomiR-136 (miR-136 agonist, 50 nM) were injected into the tumors of mice. The injections were administered twice a week for a duration of two weeks. The tumor volume was measured every other day and calculated as follows: tumor volume (V) = $(W^2 \times L)/2$. All mice were euthanized by CO_2 asphyxiation and weighed.

Immunohistochemistry

Mouse specimens were fixed with 10% formaldehyde, embedded in paraffin, and sliced into 4-μm successive sections. The obtained sections were dried, dewaxed with xylene, dehydrated with alcohol, and immersed in 3% methanol-H_2O_2 for 30 min at 37°C. Next, the sections were immersed in 0.01 M citrate buffer, heated at 95°C for 20 min, and allowed to cool down to room temperature. Subsequently, the sections were blocked with normal goat serum blocking solution for 10 min at 37°C, then incubated with primary antibodies against TWSG1 (dilution ratio of 1:200, ab57552, rabbit anti-human), Ki-67 (dilution ratio of 1:150, ab156956, mouse), matrix metalloproteinase

9 (MMP9; dilution ratio of 1:500, ab38898, rabbit), and CD34 (dilution ratio of 1:2500, ab81289, rabbit) at 4°C overnight. The following day, the sections were incubated with the corresponding biotin-labeled goat anti-rabbit secondary antibody for 10 min at room temperature. Afterwards, the sections were incubated in horseradish peroxidase-labeled *Streptomyces* ovalbumin working solution for 10 min at room temperature and stained with diaminobenzidine for 8 min in conditions void of light at room temperature. Later, the hematoxylin-stained sections were dehydrated, permeabilized, sealed, and observed under an optical microscope. The positive cells (> 25% of the total cells) were counted using the Nikon image analysis software, where obvious brown or brownish yellow granules were visualized in the cytoplasm. The number of positive cells was calculated in three non-repeated fields in each section.

Statistical analysis

SPSS 26.0 (IBM, Armonk, NY, USA) was adopted for statistical analyses. Measured data were summarized as *mean ± standard deviation*. Data between two groups were compared using the unpaired *t* test or two-way analysis of variance (ANOVA). Data among multiple groups were compared by one-way ANOVA or two-way ANOVA, while data among multiple groups at different time points were analyzed by repeated measures ANOVA, followed by Tukey's post-hoc test. The relationship between two variables was evaluated using Pearson's correlation coefficient. The survival rate was analyzed by Kaplan-Meier method and log-rank testing was adopted for univariate analysis. A value of $P < 0.05$ was considered significant.

Results

Circ_0001013 was highly expressed in GC tissues and cell lines, and correlated with poor prognosis in patients with GC

First, we explored the mechanism of circ_0001013 in GC and screened differentially expressed circRNAs in GC samples using the R software. Subsequent findings demonstrated that circ_0001013 was highly expressed in the GSE83521 microarray data (**Figure 1A**), and further exhibited the highest differential expression value (log2FC = 1.961257597, P = 0.000414929).

Furthermore, the results of RT-qPCR of the GC tissues and matched adjacent normal tissues illustrated that circ_0001013 expression was notably higher in the GC tissues relative to adjacent normal tissues (**Figure 1B**). The patients were subsequently grouped into high and low circ_0001013 expression groups using the median circ_0001013 expression as the cut-off value. Further results of Kaplan-Meier survival curve (**Figure 1C**) demonstrated that high-circ_0001013 expression patients presented with low survival rates, while low-circ_0001013 expression patients exhibited markedly increased survival rates. Moreover, circ_0001013 expression was higher in the four GC cell lines (AGS, MKN74, MKN45, and HGC-27) as compared to the normal gastric epithelial cell line GES-1 (**Figure 1D**). Together, these findings validated that circ_0001013 was up-regulated in GC tissues and cells.

Low circ_0001013 expression promoted cell cycle arrest and apoptosis, and repressed GC cell proliferation, migration, and invasion

In light of the high circ_0001013 expression patterns in GC tissues and cell lines, we investigated its function by silencing circ_0001013 in the HGC-27 GC cell line. Subsequent FISH results demonstrated that circ_0001013 was located in the cytoplasm (**Figure 2A**). The results of RT-qPCR illustrated that circ_0001013 relative expression was significantly lower in the si-circ_0001013 group than that in the control group, while there were no significant differences in the relative expression of linear 0001013 (**Figure 2B**, **2C**).

Additionally, the results of flow cytometric analysis revealed that si-circ_0001013 induced G1 arrest (**Figure 2D**) and apoptosis in the HGC-27 cells (**Figure 2E**). Colony formation assay results depicted that the si-circ_0001013 group presented with significantly fewer colonies than the NC group (**Figure 2F**). Moreover, the results of CCK-8 and EdU assays revealed that cells in the si-circ_0001013 group exhibited lower proliferative ability than those in the NC group (**Figure 2G**, **2H**). Furthermore, results of

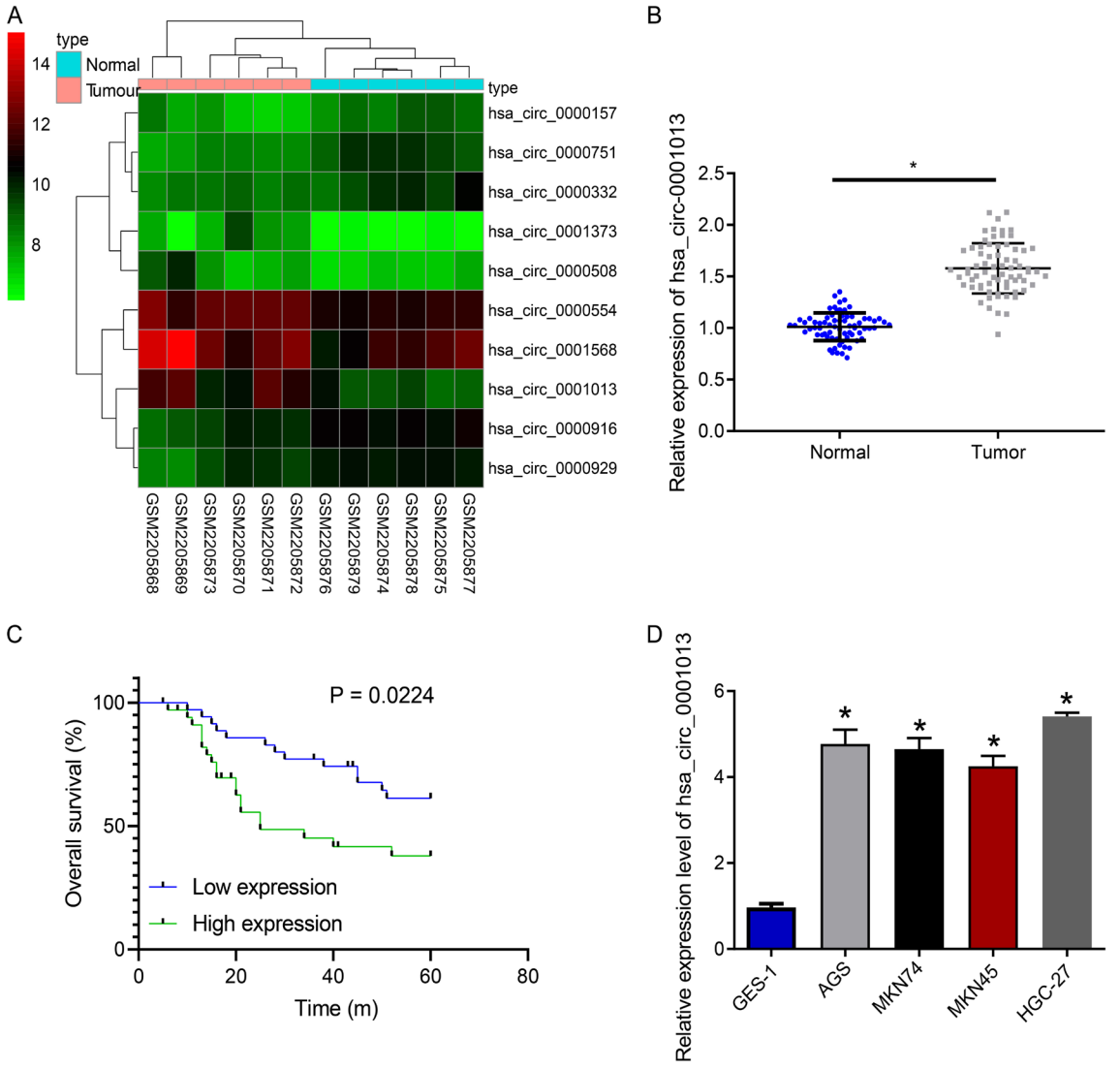

Figure 1. Circ_0001013 was upregulated in GC tissues and cell lines, which was associated with poor prognosis. (A) Heat map of the top 10 differentially expressed circRNAs in GSE83521 microarray data. The abscissa represents the sample number, the ordinate represents the differential gene, the upper right histogram represents the color scale, and each rectangle in the graph corresponds to a sample expression value. (B) RT-qPCR detection of circ_0001013 relative expression in GC and adjacent normal tissues (n = 70). (C) Kaplan-Meier survival curve. (D) RT-qPCR measurement of circ_0001013 relative expression in the GES-1 normal gastric epithelial cell line and the four GC cell lines. *$p < 0.05$ vs. adjacent normal tissues and GES-1 cells. Each cell experiment was repeated three times. Two-group data were analyzed by unpaired *t* test (B), survival analysis by Kaplan-Meier method (C), and muti-group data by one-way ANOVA (D).

scratch test and Transwell assay revealed that si-circ_0001013 inhibited GC cell migration and invasion, respectively (**Figure 2I**, **2J**).

Collectively, these findings indicated that circ_0001013 down-regulation led to decreased GC cell proliferation, migration, and invasion, and enhanced cell cycle arrest and apoptosis.

Circ_0001013 bound to miR-136 to down-regulate miR-136 expression in GC cells

We retrieved a total of 108 miRNAs that were possibly bound to hsa_circ_0001013 using the CircInteractome tool, and further downloaded 625 GC-related miRNAs from the MNDR v3.1 database, where 23 overlapping candidate miRNAs were intersected (**Figure 3A**). We next

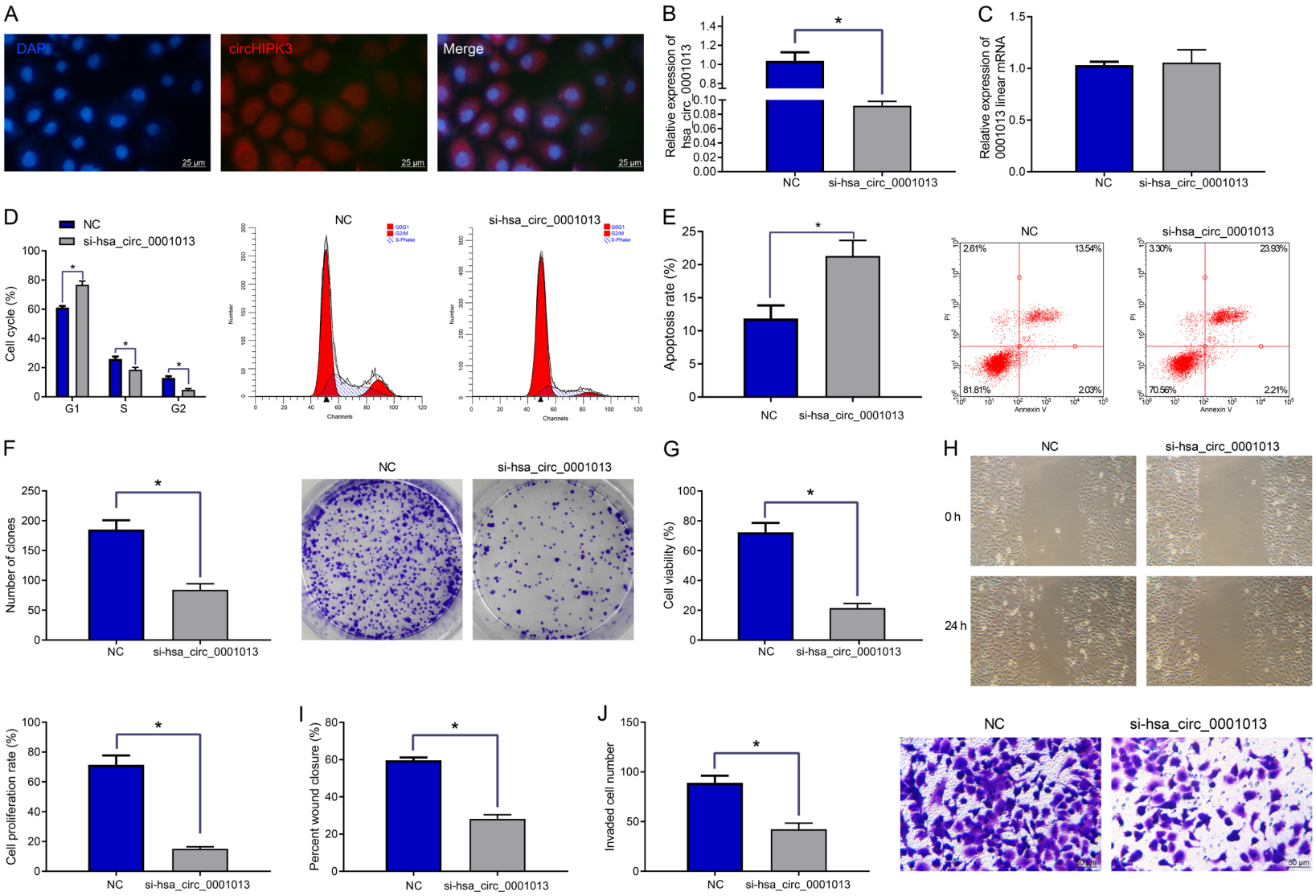

Figure 2. Low circ_0001013 expression induced GC cell cycle arrest and apoptosis and repressed GC cell proliferation, migration, and invasion. (A) FISH demonstrating that circ_0001013 was located in the cytoplasm (× 500 magnification). HGC-27 GC cells were transfected with si-circ_0001013 or NC. (B) RT-qPCR detection of circ_0001013 relative expression in HGC-27 cells. (C) RT-qPCR determination of linear circ_0001013 relative expression in HGC-27 cells. (D) Flow cytometry assessment of the distribution of HGC-27 cells in the G1, S, and G2 phases. (E) Flow cytometry detection of HGC-27 cell apoptosis. (F) HGC-27 cell colony formation. (G) CCK-8 assay of HGC-27 cell viability. (H) EdU assay measurement of HGC-27 cell proliferation. (I) Scratch test measurement of HGC-27 cell migration. (J) Transwell assay evaluation of HGC-27 cell invasion. *$P < 0.05$ vs. NC group. Each cell experiment was repeated three times. Two-group data were analyzed by unpaired *t* test (B, C, E-J), and muti-group data by one-way ANOVA (D).

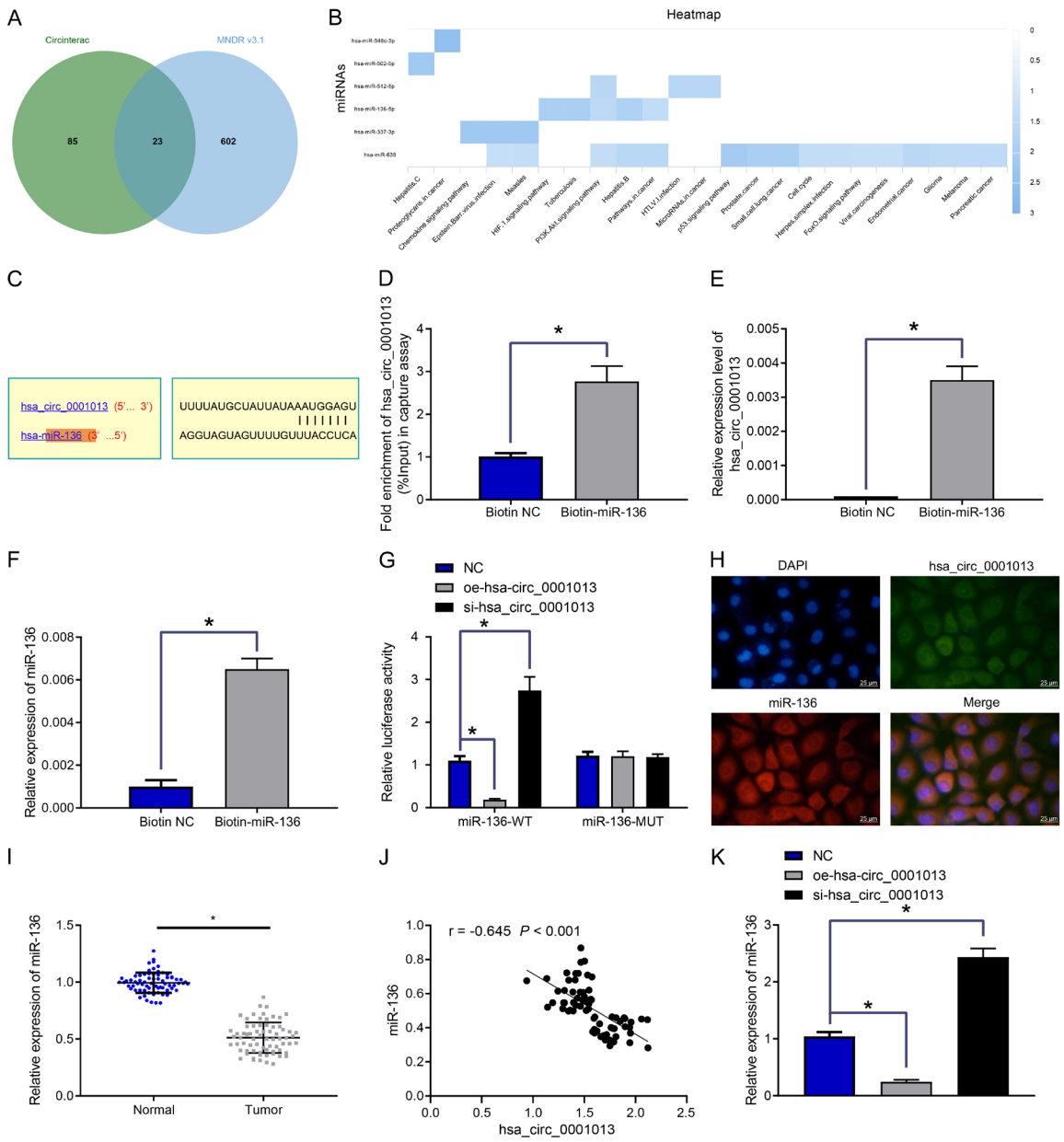

Figure 3. Circ_0001013 bound to miR-136 in GC cells. (A) Venn plot of the overlapping miRNAs between the potentially bound miRNAs of hsa_circ_0001013 in Circinteractome database and the GC-associated miRNAs in the MNDR v3.1 database. (B) Heatmap of the KEGG pathway involving miRNAs in the miRPathDB v2.0 database, where darker blue indicates higher the-log10 (*p*-value). (C) Targeted binding of circ_0001013 to miR-136. (D) RT-qPCR detection of circ_0001013 captured by biotin-coupled miR-136. (E) RT-qPCR detection of circ_0001013 enriched by specific probes. (F) RT-qPCR detection of miR-136 enrichment by circ_0001013-specific probe. (G) Dual-luciferase reporter assay verification of the binding relationship between circ_0001013 and miR-136. (H) FISH detection of circ_0001013 and miR-136 co-localization (× 400 magnification). (I) RT-qPCR estimation of miR-136 expression in GC tissues and the adjacent normal tissues. (J) Correlation analysis of circ_0001013 and miR-136 expression in GC tissues. (K) miR-136 expression in AGS cells after circ_0001013 silencing or overexpression. *$P < 0.05$. Each cell experiment was repeated three times. Two-group data were analyzed by unpaired *t* test (DEFI), muti-group data by one-way ANOVA (K) or two-way ANOVA (G), and correlation between two variables by Pearson correlation coefficient (J).

analyzed the KEGG pathways that miRNAs were implicated in through the miRPathDB v2.0 database, and the subsequent results demonstrated that miR-136 and miR-638 were involved in cancer signaling (**Figure 3B**). Thereafter, we queried the expression patterns of miR-136 and miR-638 in dataset GSE16579 through the deepBase v3.0 database, and dis-

Table 2. The data of miR-136 in the deepBase v3.0 database in Dataset GSE16579 (miRNA expression of human cancer and mouse cell lines)

ID	Name	Chromosome	Start	End	Type	Strand	Samples	Expression
MI0000475	hsa-mir-136	chr14	1.01E+08	1.01E+08	miRNA	+	6	5.320723

covered that miR-136 was expressed and miR-638 was not expressed (**Table 2**). Accordingly, miR-136 was selected for further experimentation. Additional bioinformatic database CircInteractome analysis identified the presence of binding sites between circ_0001013 and miR-136 (**Figure 3C**). Moreover, pull-down assay and RT-qPCR revealed that miR-136 was significantly pulled down by the circRNA probe. Biotin-labeled miR-136 and its mutant mimic further indicated that miR-136-Wt captured more circRNA in the HGC-27 cells over-expressing circRNA (**Figure 3D-F**). Results of luciferase reporter assay showed that the miR-136 mimic markedly reduced the luciferase activity of the complete circRNA sequence, while that of miR-136-Mut was unaffected (**Figure 3G**).

Additional FISH experimentation demonstrated that circ_0001013 and miR-136 were co-located in the cytoplasm (**Figure 3H**). Moreover, miR-136 was poorly expressed in GC tissues (**Figure 3I**). Correlation analysis further revealed that circ_0001013 expression was negatively correlated with miR-136 expression in GC tissues (**Figure 3J**). Furthermore, miR-136 was decreased in response to circ_0001013 over-expression, while being increased following circ_0001013 silencing in AGS cells (**Figure 3K**), highlighting that circ_0001013 could bind to and negatively regulate miR-136 in GC cells.

miR-136 reversed the cancer-promoting effect of circ_0001013 on GC cells

Thereafter, we evaluated the function of miR-136 in GC by co-transfecting AGS cells with miR-136 mimic and circ_0001013 plasmids and detecting the GC cell migration, invasion, and the cell cycle and apoptosis. Subsequent findings revealed that circ_0001013 over-expression augmented AGS cell migration (**Figure 4A**), invasion (**Figure 4B**), and the number of cells arrested at the G2 phase (**Figure 4C**), and diminished apoptosis (**Figure 4D**), while these effects were normalized by further over-expression of miR-136. Altogether, these findings indicated that miR-136 over-expression abolished the oncogenic effect of circ_0001013 on GC.

Circ_0001013 up-regulated the expression of the miR-136 target gene TWSG1

Prediction results of miRDB, starBase, microT, and mirDIP databases revealed a total of 225, 2649, 434, and 187 potential target genes of miR-136, respectively. GEPIA predicted 3741 genes that could be significantly highly expressed in GC samples, and 12 candidate genes were obtained using the intersection of the predicted target genes and the differentially highly expressed genes in GC samples: *HOXC10*, *CBX4*, *ZNF710*, *CAMSAP2*, *MTPN*, *ZNF148*, *XIAP*, *ANXA4*, *MBNL3*, *DCAF7*, *TNRC18*, and *TWSG1* (**Figure 5A**). Moreover, GO enrichment analysis demonstrated that the 12 candidate genes were involved in biological processes (**Figure 5B**). According to the results, BMP-related signaling pathways occupied more entries in the network, and TWSG1 and XIAP genes were involved in these two pathways. Based on further correlation analysis of expression and survival in GC patients using KMplot database, high TWSG1 expression was found to be significantly negatively correlated with survival in GC patients (**Figure 5C**), while XIAP expression was not significantly correlated with survival in GC patients (**Figure 5D**). Accordingly, TWSG1 was selected as the focus of our study. Furthermore, GEPIA analysis illustrated that *TWSG1* was highly expressed in GC samples (**Figure 5E**), and the starBase database indicated that miR-136 had a binding site with *TWSG1* in GC cells (**Figure 5F**).

Results of dual-luciferase reporter assay validated that miR-136 mimic strongly diminished TWSG1-Wt luciferase activity, while that of TWSG1-Mut was unaltered (**Figure 5G**). Additional RT-qPCR results illustrated that *TWSG1* expression was remarkably higher in GC tissues relative to adjacent normal tissues (**Figure 5H**). Correlation analysis further revealed a positive correlation between the expression of circ_0001013 and *TWSG1* (**Figure 5I**).

Thereafter, we determined whether circ_0001013 could regulate the target gene *TWSG1* to exert its anti-tumor effect by miR-136. Sub-

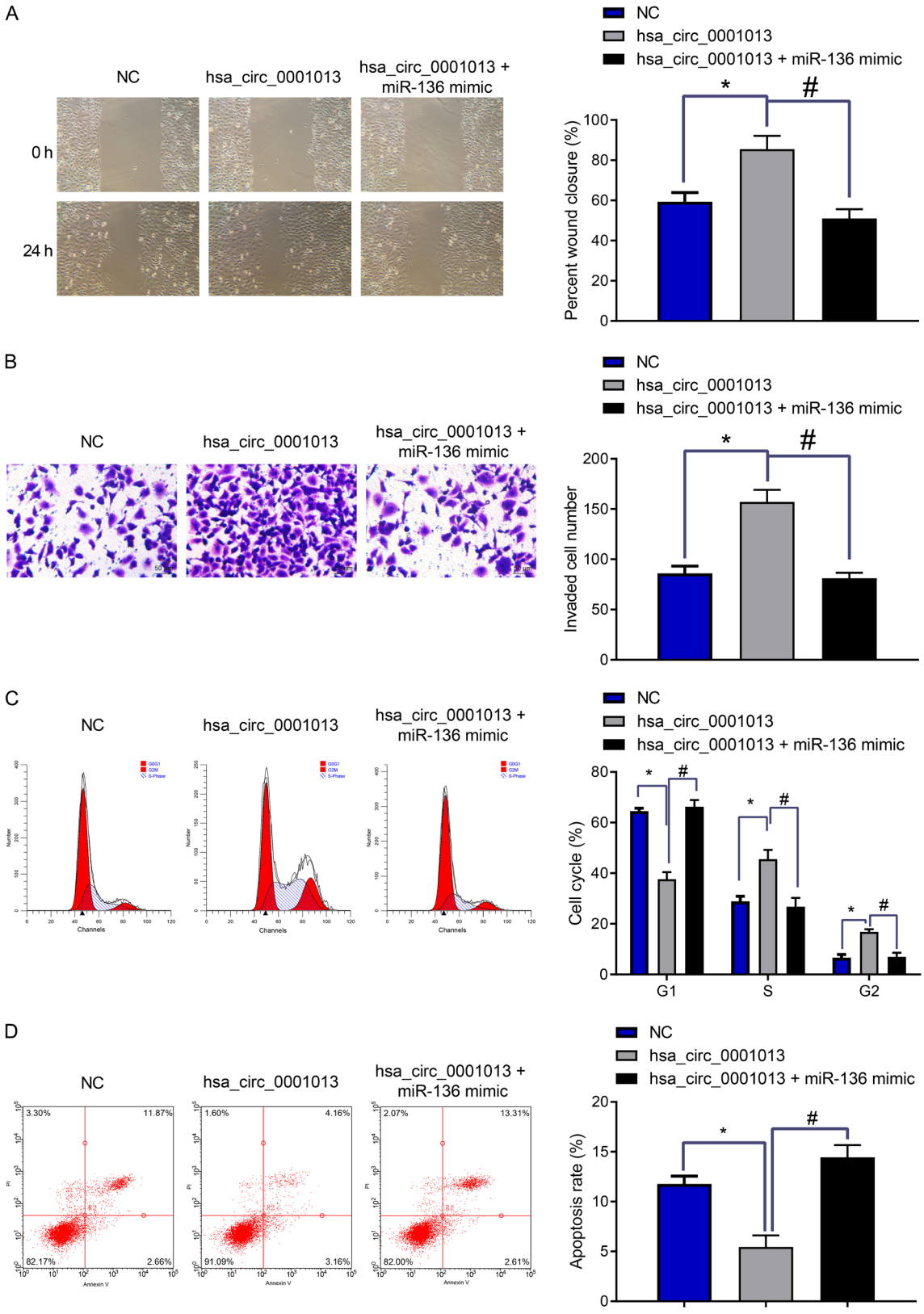

Figure 4. miR-136 inhibits GC cell migration and invasion to counteract the cancer-promoting effect of circ_0001013. AGS cells were transfected with NC, circ_0001013, or circ_0001013 + miR-136 mimic. (A) Scratch test measurement of AGS cell migration. (B) Transwell assay determination of AGS cell invasive ability. (C) Flow cytometry detection of the AGS cell cycle. (D) Flow cytometry measurement of AGS cell apoptosis. *$P < 0.05$, #$P < 0.05$. Each cell experiment was repeated three times. Muti-group data were analyzed by one-way ANOVA (K) or two-way ANOVA (G).

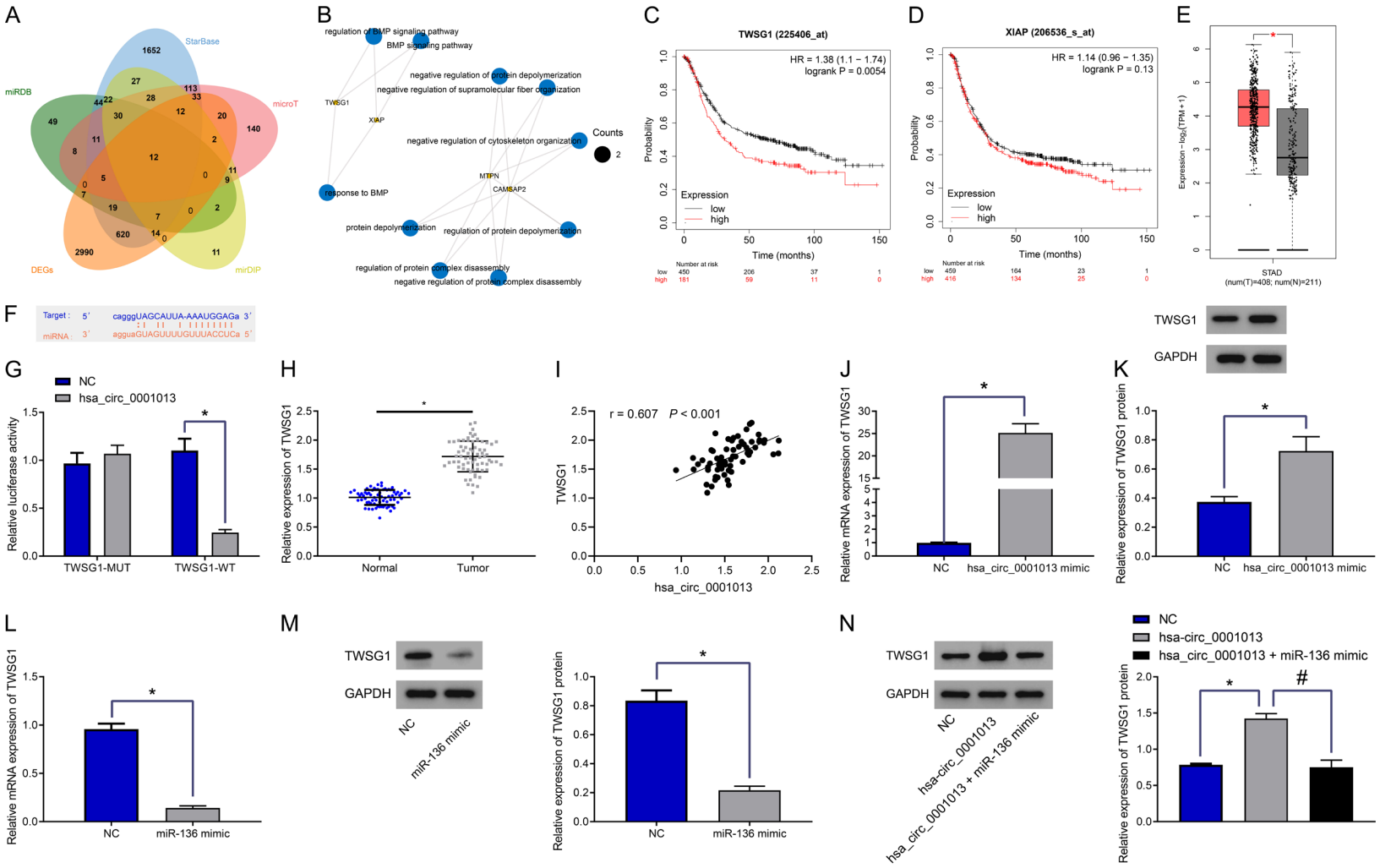

Figure 5. Circ_0001013 caused *TWSG1* upregulation by binding to miR-136. (A) Venn map of the target genes of miR-136 predicted by miRDB, starBase, microT, and mirDIP and the upregulated genes in the GC samples. (B) Visualized network of the top 10 entries of the GO enrichment analysis results, with blue for GO entries and yellow for gene. (C) Survival curve of TWSG1 in GC. (D) Survival curve of XIAP in GC. (E) *TWSG1* expression in GC samples in the TCGA database. (F) The miR-136 and *TWSG1* binding sites predicted by starBase. (G) Dual-luciferase reporter assay verification of the relationship between miR-136 and TWSG1. (H) RT-qPCR detection of TWSG1 expression in GC tissues and the adjacent normal tissues. (I) Correlation analysis of circ_0001013 and TWSG1 expression in GC tissues. (J) RT-qPCR detection of *TWSG1* mRNA expression in cells overexpressing circ_0001013. (K) Western blot assay determination of TWSG1 protein expression in cells overexpressing circ_0001013. (L) RT-qPCR determination of *TWSG1* mRNA expression in cells treated with miR-136 mimic. (M) Western blot assay of TWSG1 protein expression in cells treated with miR-136 mimic. (N) Western blot assay detection of TWSG1 protein expression in cells after co-transfection with circ_0001013 and miR-136 mimic. *$P < 0.05$, #$P < 0.05$. Each cell experiment was repeated three times. Two-group data were analyzed by two-way ANOVA (G) or unpaired *t* test (HJKLM), muti-group data by one-way ANOVA (N), and correlation between two variables by Pearson correlation coefficient (I).

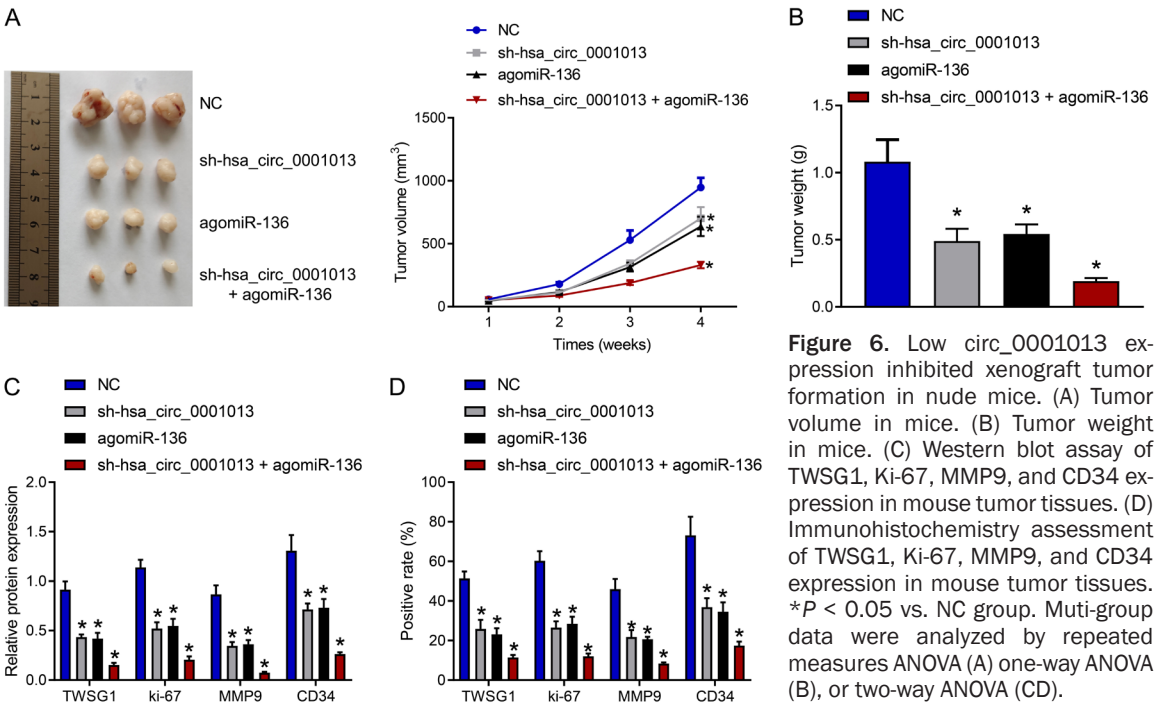

Figure 6. Low circ_0001013 expression inhibited xenograft tumor formation in nude mice. (A) Tumor volume in mice. (B) Tumor weight in mice. (C) Western blot assay of TWSG1, Ki-67, MMP9, and CD34 expression in mouse tumor tissues. (D) Immunohistochemistry assessment of TWSG1, Ki-67, MMP9, and CD34 expression in mouse tumor tissues. *$P < 0.05$ vs. NC group. Muti-group data were analyzed by repeated measures ANOVA (A) one-way ANOVA (B), or two-way ANOVA (CD).

sequent results of RT-qPCR and western blot assay illustrated that circ_0001013 over-expression enhanced the mRNA and protein levels of TWSG1 (**Figure 5J**, **5K**), while opposing trends were noted following miR-136 mimic transfection (**Figure 5L**, **5M**). These findings validated *TWSG1* as a direct target of miR-136.

TWSG1 expression was additionally evaluated by co-transfection of circ_0001013 and miR-136 mimic. circ_0001013 over-expression partially rescued the inhibitory role of miR-136 on *TWSG1* expression (**Figure 5N**).

Altogether, these findings indicated that circ_0001013 bound to miR-136 to up-regulate *TWSG1* expression in GC cells.

Knockdown of circ_0001013 inhibited xenograft tumorigenesis in nude mice

Lastly, we investigated whether circ_0001013 over-expression could affect tumor growth *in vivo*. Xenograft mouse models were established by subcutaneous injection of equal amounts of AGS cells (n = 8 mice per group). After 10 days, when the tumor volume was 100 mm^3, lentivirus containing sh-circ_0001013 (1×10^9 TU/ml, 50 μl) alone, or combined with agomiR-136 (miR-136 agonist, 50 nM) were injected into the tumor twice a week for 2 weeks to construct the sh-circ_0001013, agomiR-136, and sh-circ_0001013 + agomiR-136 groups. Tumor volume and weight were measured every other week, which revealed that compared to the NC group, the average tumor volume and weight were markedly reduced in the agomiR-136 and sh-circ_0001013 groups (**Figure 6A**, **6B**), wherein the decline was most pronounced in the sh-circ_0001013 + agomiR-136 group in contrast to the sh-circ_0001013 group. Additionally, results of western blot assay demonstrated that TWSG1 protein expression was decreased in the agomiR-136 and sh-circ_0001013 groups (**Figure 6C**), while TWSG1, Ki-67, MMP9, and CD34 protein expression was most substantially reduced in the sh-circ_0001013 + agomiR-136 group. Immunohistochemical analysis showed that TWSG1, Ki-67, MMP9, and CD34 were markedly decreased after circ_0001013 silencing and miR-136 over-expression (**Figure 6D**).

Collectively, these findings illustrated that circ_0001013 down-regulation repressed xenograft tumorigenesis in nude mice.

Discussion

A vast majority of gastric cancer (GC) patients are often diagnosed at an advanced stage,

which leads to poor prognosis and dismal outcome [15]. Therefore, it is imperative to advance our understanding of the molecular mechanism underlying GC development. The obtained findings indicated that circ_0001013 overexpression enhanced *TWSG1* expression by binding to miR-136, thereby promoting GC cell proliferation, migration, and invasion and inhibiting their apoptosis.

Aberrant expression of numerous circRNAs is widely implicated in a plethora of GC processes, including cell proliferation, apoptosis, migration, and invasion of GC cells [16]. For instance, hsa_circ-0000670 expression is highly expressed in GC tissues and cell lines, and its up-regulation exerts an enhancing effect on GC cell proliferative, invasive, and migration capabilities [17]. Similarly, circNRIP1 was overexpressed in GC tissues, whereas silencing of circNRIP1 led to diminished GC cell proliferation, migration, and invasion [18]. In addition, a prior study documented up-regulation of hsa_circ_0000467 in GC tissues and cell lines, while its down-regulation was associated with diminished GC cell proliferation, invasion, and cell cycle entry [19]. Further elaborating the association of circRNAs with GC, circ_CACTIN was up-regulated in GC tissues and cells, and its knockdown triggered the inhibition of GC cell proliferation, migration, and invasion [20]. Much in accordance with the above-mentioned evidence, our microarray analysis predicted up-regulation of circ_0001013 expression in GC samples, and the finding was verified by RT-qPCR detection in GC tissues and cells. In addition, findings of subsequent functional cell experimentation revealed that silencing of circ_0001013 brought about a reduction in GC cell proliferation, invasion, and migration, and further augmented apoptosis and cell cycle arrest. Altogether, the aforementioned findings and evidence highlight the oncogenic role of circ_0001013 in GC development.

circRNAs are known to function as competing endogenous RNAs or miRNA sponges to bind miRNAs through a miRNA response element, thereby negatively orchestrating miRNA activity [21]. In a similar light, we discovered that circ_0001013 was capable of binding to miR-136, and further down-regulated miR-136 expression in GC cells. In addition, our findings illustrated that miR-136 was poorly expressed in GC tissues, whereas over-expression of miR-136 in GC cells led to reduced cell cycle entry, proliferation, invasion, and migration, while simultaneously enhancing GC apoptosis. Concordant with our discovery, the study performed by Yu L *et al.* indicated that miR-136 expression is down-regulated in GC cells, whereas enforced miR-136 expression contributed to increased GC cell apoptosis by targeting AEG-1 and BCL2 [11]. Consistently, another report demonstrated that up-regulation of miR-136 led to repression of GC cell proliferation, migration, and invasion [22]. Furthermore, Jin *et al.* noted that miR-136 was poorly expressed in colorectal cancer (CRC) tissues and cell lines, while ectopically expressed miR-136 reduced CRC cell proliferation, migration, and invasion and caused G0/G1 arrest [23]. Down-regulation of miR-136 was also previously detected in endometrial cancer (EC) tissues and cells, and unsurprisingly, miR-136 up-regulation was correlated with diminished EC cell proliferation, migration, and invasion [24]. Collectively, these findings and evidence confirm the tumor-suppressive ability of miR-136 in GC development.

Furthermore, miRNAs possess the ability to repress the expression of target mRNAs by binding to their 3'UTR, thereby participating in the pathological processes of numerous human diseases, including cancers [25]. Herein, findings from bioinformatics analyses, dual-luciferase reporter assay, and RT-qPCR in our study revealed that miR-136 bound to the *TWSG1* 3'UTR to decrease the expression of *TWSG1* in GC cells. Further experimentation demonstrated that TWSG1 was up-regulated in GC tissues, while the above-mentioned effects of miR-136 over-expression on GC cell proliferation, invasion, migration, cell cycle arrest and apoptosis were exerted by down-regulation of *TWSG1*. Consistent with this, *TWSG1* was previously shown to be up-regulated in PTC tissues, such that *TWSG1* knockdown repressed PTC cell migration, invasion, and proliferation [12]. Additionally, the efforts of Liu *et al.* detailed that *TWSG1* expression was substantially augmented in glioma tissues relative to normal brain tissues, and that *TWSG1* up-regulation was associated with enhanced glioma cell proliferation [26].

In conclusion, the current study identified a novel circRNA, circ_0001013, that augmented

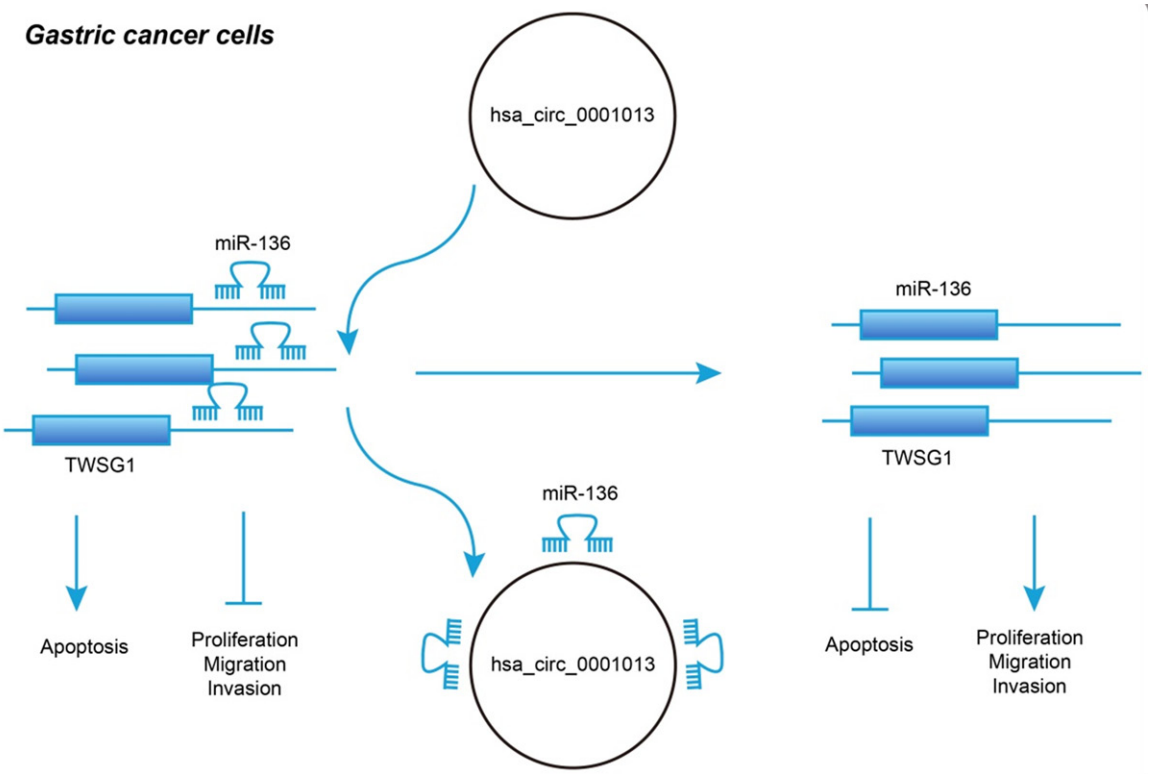

Figure 7. Schematic diagram of the mechanism by which circ_0001013 affects GC. In GC cells, circ_0001013 binds to miR-136, which negatively targets *TWSG1*. High circ_0001013 expression decreases miR-136 expression to up-regulate *TWSG1*, which promotes GC cell proliferation, migration, and invasion and inhibits GC apoptosis.

GC cell proliferation, migration, and invasion, while decreasing their apoptosis by binding to miR-136 and positively regulating *TWSG1* expression (**Figure 7**). Our findings shed light on the critical roles of the circ_0001013-miR-136-TWSG1 axis in GC, and pave the way for novel targets against GC.

Acknowledgements

This work was supported by the science and technology planning project of Jiaxing City (No. 2017BY18014).

Disclosure of conflict of interest

None.

Address correspondence to: Xiaoguang Wang, Faculty of Graduate Studies, Zhejiang Chinese Medical University, No, 548, Binwen Road, Hangzhou 310053, Zhejiang, P. R. China. Tel: +86-0573-8208-0930; E-mail: xiaoguangwangs@163.com; Biwen Hu, Department of Surgery, The Second Affiliated Hospital of Jiaxing University, No. 397, Huangcheng North Road, Jiaxing 314000, Zhejiang, P. R. China. E-mail: hbw-1979@163.com

References

[1] Bray F, Ferlay J, Soerjomataram I, Siegel RL, Torre LA and Jemal A. Global cancer statistics 2018: GLOBOCAN estimates of incidence and mortality worldwide for 36 cancers in 185 countries. CA Cancer J Clin 2018; 68: 394-424.

[2] Smyth EC, Nilsson M, Grabsch HI, van Grieken NC and Lordick F. Gastric cancer. Lancet 2020; 396: 635-648.

[3] Johnston FM and Beckman M. Updates on management of gastric cancer. Curr Oncol Rep 2019; 21: 67.

[4] Coutzac C, Pernot S, Chaput N and Zaanan A. Immunotherapy in advanced gastric cancer, is it the future? Crit Rev Oncol Hematol 2019; 133: 25-32.

[5] Molina-Castro S, Pereira-Marques J, Figueiredo C, Machado JC and Varon C. Gastric cancer: basic aspects. Helicobacter 2017; 22.

[6] Wei L, Sun J, Zhang N, Zheng Y, Wang X, Lv L, Liu J, Xu Y, Shen Y and Yang M. Noncoding

RNAs in gastric cancer: implications for drug resistance. Mol Cancer 2020; 19: 62.
[7] Cheng J, Zhuo H, Xu M, Wang L, Xu H, Peng J, Hou J, Lin L and Cai J. Regulatory network of circRNA-miRNA-mRNA contributes to the histological classification and disease progression in gastric cancer. J Transl Med 2018; 16: 216.
[8] Cao J, Zhang X, Xu P, Wang H, Wang S, Zhang L, Li Z, Xie L, Sun G, Xia Y, Lv J, Yang J and Xu Z. Circular RNA circLMO7 acts as a microRNA-30a-3p sponge to promote gastric cancer progression via the WNT2/beta-catenin pathway. J Exp Clin Cancer Res 2021; 40: 6.
[9] Niu Q, Dong Z, Liang M, Luo Y, Lin H, Lin M, Zhong X, Yao W, Weng J and Zhou X. Circular RNA hsa_circ_0001829 promotes gastric cancer progression through miR-155-5p/SMAD2 axis. J Exp Clin Cancer Res 2020; 39: 280.
[10] Li J, Yang Y, Xu D and Cao L. hsa_circ_0023409 accelerates gastric cancer cell growth and metastasis through regulating the IRS4/PI3K/AKT pathway. Cell Transplant 2021; 30: 963689720975390.
[11] Yu L, Zhou GQ and Li DC. MiR-136 triggers apoptosis in human gastric cancer cells by targeting AEG-1 and BCL2. Eur Rev Med Pharmacol Sci 2018; 22: 7251-7256.
[12] Xia S, Ji R, Xu Y, Ni X, Dong Y and Zhan W. Twisted gastrulation BMP signaling modulator 1 regulates papillary thyroid cancer cell motility and proliferation. J Cancer 2017; 8: 2816-2827.
[13] Gautier L, Cope L, Bolstad BM and Irizarry RA. Affy--analysis of Affymetrix GeneChip data at the probe level. Bioinformatics 2004; 20: 307-315.
[14] Smyth GK. Linear models and empirical bayes methods for assessing differential expression in microarray experiments. Stat Appl Genet Mol Biol 2004; 3: Article3.
[15] Sukri A, Hanafiah A, Mohamad Zin N and Kosai NR. Epidemiology and role of helicobacter pylori virulence factors in gastric cancer carcinogenesis. APMIS 2020; 128: 150-161.
[16] Li R, Jiang J, Shi H, Qian H, Zhang X and Xu W. CircRNA: a rising star in gastric cancer. Cell Mol Life Sci 2020; 77: 1661-1680.
[17] Liu P, Cai S and Li N. Circular RNA-hsa-circ-0000670 promotes gastric cancer progression through the microRNA-384/SIX4 axis. Exp Cell Res 2020; 394: 112141.
[18] Zhang X, Wang S, Wang H, Cao J, Huang X, Chen Z, Xu P, Sun G, Xu J, Lv J and Xu Z. Circular RNA circNRIP1 acts as a microRNA-149-5p sponge to promote gastric cancer progression via the AKT1/mTOR pathway. Mol Cancer 2019; 18: 20.
[19] Mo WL, Jiang JT, Zhang L, Lu QC, Li J, Gu WD, Cheng Y and Wang HT. Circular RNA hsa_circ_0000467 promotes the development of gastric cancer by competitively binding to MicroRNA miR-326-3p. Biomed Res Int 2020; 2020: 4030826.
[20] Zhang L, Song X, Chen X, Wang Q, Zheng X, Wu C and Jiang J. Circular RNA CircCACTIN promotes gastric cancer progression by sponging MiR-331-3p and regulating TGFBR1 expression. Int J Biol Sci 2019; 15: 1091-1103.
[21] Verduci L, Strano S, Yarden Y and Blandino G. The circRNA-microRNA code: emerging implications for cancer diagnosis and treatment. Mol Oncol 2019; 13: 669-680.
[22] Yu X, Xiao W, Song H, Jin Y, Xu J and Liu X. CircRNA_100876 sponges miR-136 to promote proliferation and metastasis of gastric cancer by upregulating MIEN1 expression. Gene 2020; 748: 144678.
[23] Jin C, Wang A, Liu L, Wang G and Li G. Hsa_circ_0136666 promotes the proliferation and invasion of colorectal cancer through miR-136/SH2B1 axis. J Cell Physiol 2019; 234: 7247-7256.
[24] Shi Y, Jia L and Wen H. Circ_0109046 promotes the progression of endometrial cancer via regulating miR-136/HMGA2 axis. Cancer Manag Res 2020; 12: 10993-11003.
[25] Ali Syeda Z, Langden SSS, Munkhzul C, Lee M and Song SJ. Regulatory mechanism of microrna expression in cancer. Int J Mol Sci 2020; 21: 1723.
[26] Liu Z and Li H. Twisted gastrulation signaling modulator 1 promotes the ability of glioma cell through activating Akt pathway. Neuroreport 2021; 32: 198-205.